International Journal of Minerals, Metallurgy and Materials
Volume 22, Number 11, November 2015, Page 1219
DOI: 10.1007/s12613-015-1188-6

Morphology characterization of periclase–hercynite refractories by reaction sintering

Peng Jiang[1)], *Jun-hong Chen*[1)], *Ming-wei Yan*[1)], *Bin Li*[1)], *Jin-dong Su*[1)], *and Xin-mei Hou*[2)]

1) School of Materials Science and Engineering, University of Science and Technology Beijing, Beijing 100083, China

2) Collaborative Innovation Center of Steel Technology, University of Science and Technology Beijing, Beijing 100083, China

(Received: 15 May 2015; revised: 28 July 2015; accepted: 28 July 2015)

Abstract: A periclase–hercynite brick was prepared via reaction sintering at 1600°C for 6 h in air using magnesia and reaction-sintered hercynite as raw materials. The microstructure development of the periclase–hercynite brick during sintering was investigated using X-ray diffraction, X-ray photoelectron spectroscopy, and scanning electron microscopy in combination with energy-dispersive X-ray spectroscopy. The results show that during sintering, Fe^{2+}, Fe^{3+} and Al^{3+} ions in hercynite crystals migrate and react with periclase to form $(Mg_{1-x}Fe_x)(Fe_{2-y}Al_y)O_4$ spinel with a high Fe/Al ratio. Meanwhile, Mg^{2+} in periclase crystals migrates into hercynite crystals and occupies the oxygen tetrahedron vacancies. This Mg^{2+} migration leads to the formation of $(Mg_{1-u}Fe_u)(Fe_{2-v}Al_v)O_4$ spinel with a lower Fe/Al ratio and results in Al^{3+} remaining in hercynite crystals. Cation diffusion between periclase and hercynite crystals promotes the sintering process and results in the formation of a microporous structure.

Keywords: refractories; periclase; hercynite; sintering; morphology; diffusion

1. Introduction

Magnesia–chrome bricks have been widely used in cement rotary kilns for many years because of their excellent properties, which include good corrosion resistance and good coating adhesion stability [1–2]. However, because of environmental concerns, many countries have passed legislation forbidding the use of chrome bricks. Therefore, attention has been directed toward the development of chrome-free refractories to replace magnesia–chrome refractories [3–11]. In recent years, the use of periclase–hercynite refractories based on hercynite ($FeO{\cdot}Al_2O_3$) and periclase has become an important trend in the development of chrome-free refractories; such periclase–hercynite refractories have been successfully used as a substitute for magnesia–chrome bricks in the burning zone of cement rotary kilns [12–15].

Recent research has been focused mainly on the preparation of periclase–hercynite refractories using fused hercynite as a raw material. For instance, Guo and Nievoll [14] synthesized magnesia–hercynite refractories from high-purity magnesia and fused hercynite. In their study, a spinel layer was formed on the surface of fused hercynite crystals. Liu *et al*. [15] investigated the composition and structure of the composite spinel made from magnesia and fused hercynite at high temperatures. They observed that hercynite was initially decomposed into γ-Al_2O_3 and γ-Fe_2O_3, which reacted with MgO to form $MgO{\cdot}Al_2O_3$ and $MgO{\cdot}Fe_2O_3$, respectively. Then, γ-Fe_2O_3 dissolved into $MgO{\cdot}Al_2O_3$ or γ-Al_2O_3 dissolved into $MgO{\cdot}Fe_2O_3$ to form a composite spinel such as $MgFe_xAl_{2-x}O_4$ or $MgFe_2O_4$. Compared with the bricks synthesized from fused hercynite and magnesia, the bricks prepared from reaction sintering using hercynite and magnesia as raw materials exhibited a better kiln-coating ability and better thermal shock resistance because of their high reactivity.

In this study, a periclase–hercynite brick was prepared by reaction sintering at 1600°C for 6 h in air using magnesia and reaction-sintered hercynite as raw materials. Given that the performance of the periclase–hercynite brick is mainly attributable to its chemical composition, microstructure, and element distribution, we investigated the element distribution and microstructure evolution to establish a foundation

Corresponding author: Jun-hong Chen, E-mail: cjh2666@126.com; Xin-mei Hou, E-mail: houxinmei@ustb.edu.cn

for the practical application of periclase–hercynite refractories.

2. Experimental

High-purity sintered magnesia (97.3wt% MgO, 1.35wt% CaO, and 1.25wt% SiO_2) and pre-synthesized reaction-sintered hercynite (43wt% Fe_2O_3 and 57wt% Al_2O_3) were adopted as raw materials. Methyl cellulose was used as a binder. High-purity sintered magnesia (0–5 mm) and hercynite (0–5 mm) were wet-mixed in a mass ratio of 90:10 and then pressed into green bricks with dimensions of 65 mm × 110 mm × 230 mm under a pressure of 200 MPa. The dried green bricks were subsequently sintered at 1600°C for 6 h in air.

The phase and microstructure of the sample before and after sintering were characterized using X-ray diffraction (XRD) and scanning electron microscopy (SEM) in combination with energy-dispersive X-ray spectroscopy (EDS). XRD measurements were performed on a Rigaku D/Max 2200PC diffractometer (Rigaku Corp., Tokyo, Japan); the samples were scanned over a 2θ range of 10° to 90°. SEM observations were performed using a Quanta 200 (FEI, The Netherlands) scanning electron microscope equipped with an energy-dispersive X-ray spectrometer (INCA250 Oxford Instruments, UK). The valence of Fe in the periclase phase of the sintered bricks was characterized with an X-ray photoelectron spectroscope (ESCALAB 250Xi, Thermo Fisher Scientific).

3. Results and discussion

3.1. XPS and XRD analyses

Fig. 1 shows the XRD pattern of the periclase–hercynite brick sintered at 1600°C for 6 h in air. Almost all the characteristic peaks correspond to the phases of periclase and composite spinels containing Mg, Fe, Al and O. The characteristic peaks in the magnified 2θ region between 29° and 40° shown in the inset of Fig. 1 further confirm the existence of a composite spinel ($(Mg_{1-x}Fe_x)(Fe_{2-y}Al_y)O_4$) with a high Fe/Al ratio.

The iron state in the magnesia crystal was investigated by X-ray photoelectron spectroscopy (XPS). Fig. 2 shows the XPS spectrum of magnesia grains in the sintered bricks. As analyzed using peak-deconvolution software, peaks at 724.6 eV and 710.8 eV correspond to the binding energies of Fe $2p_{1/2}$ and Fe $2p_{3/2}$ respectively. A satellite peak at 718.8 eV was also detected, indicating that iron exists in the form of Fe^{3+} in magnesia, which is in consistent with results reported in Ref. [16]. Fe^{3+} ions are mainly transformed from Fe^{2+} ions in hercynite and may diffuse into crystalline magnesia. This possibility will be further discussed in the following section.

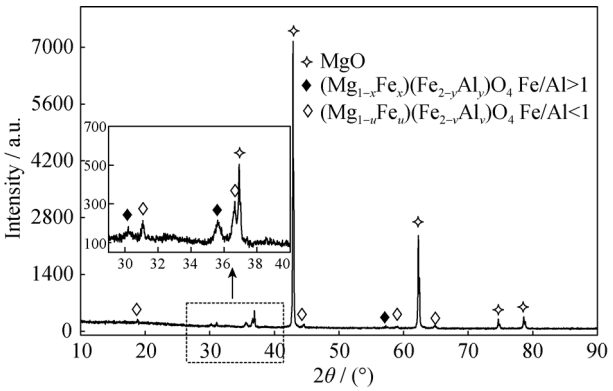

Fig. 1. XRD pattern of the periclase–hercynite brick sintered at 1600°C for 6 h in air.

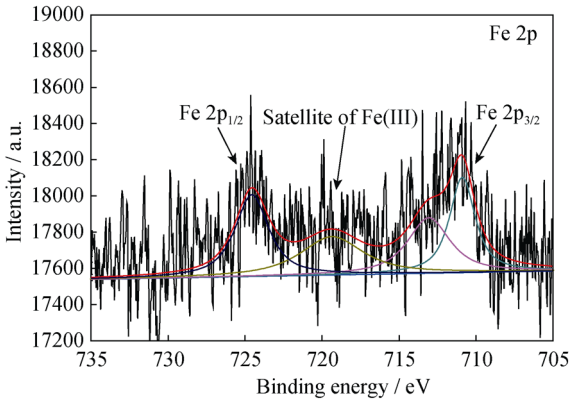

Fig. 2. XPS pattern of magnesia grains in the sintered periclase–hercynite brick.

3.2. Morphology of the periclase–hercynite brick before and after sintering

Figs. 3(a) and 3(b) indicate the morphology of the periclase–hercynite brick before sintering. The white grains are hercynite (Area 1), and the gray grains (Area 2) are sintered magnesia. EDS analysis indicates that no other elements were present inside crystalline magnesia. Impurities such as Si and Ca were mainly located at the periclase crystal boundary (Area 3).

The morphology of the periclase–hercynite brick after sintering is shown in Figs. 3(c) and 3(d). After the brick was sintered, cavities were clearly observed, especially in large hercynite crystals (Fig. 3(c)); these cavities lead to the formation of a shell microstructure. Some bright spots were detected in the inner part of the periclase crystals of magnesia grains that contact with hercynites. EDS analysis shows

that the periclase boundaries comprise Mg, Ca, Si, Fe, Al, and O (Area 4), whereas both the shells and the bright spots are composed of Al, Mg, Fe, and O (areas 5 and 6). Compared with the green brick before sintering (Figs. 3(a) and 3(b)), the sintered brick contains more micropores in its matrix. On the basis of SEM and EDS results (Table 1), we concluded that Fe mainly existed in crystalline periclase, whereas Al mainly remained in the matrix. Combined XRD (Fig. 1) and XPS (Fig. 2) results reveal that the shells are composed of spinel solid solution with a small amount of dissolved Fe ions ($(Mg_{1-u}Fe_u)(Fe_{2-v}Al_v)O_4$), whereas the bright spots are composed of $(Mg_{1-x}Fe_x)(Fe_{2-y}Al_y)O_4$) spinel.

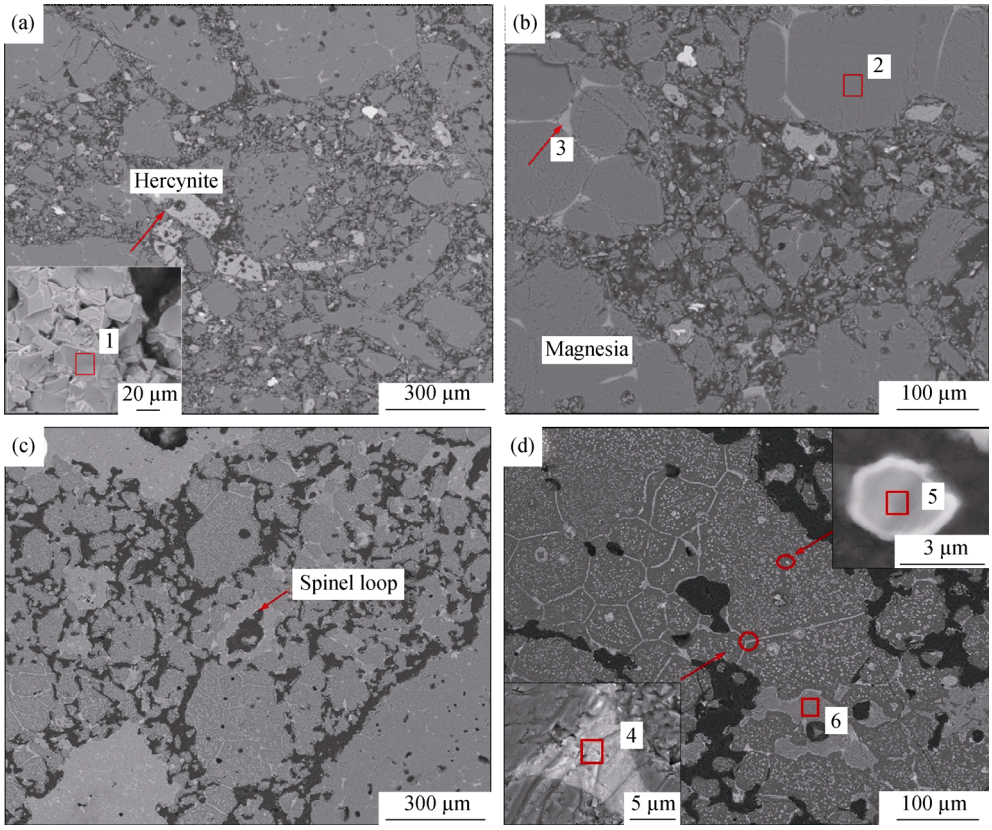

Fig. 3. Morphology of periclase–hercynite brick (a,b) before and (c,d) after sintering at 1600°C for 6 h in air.

Table 1. EDS analysis results for areas in Fig. 3 at%

Microzones	Mg	Fe	Al	Ca	Si	O
1	—	15.83	32.76	—	—	51.41
2	50.00	—	—	—	—	50.00
3	18.08	—	—	14.52	11.60	55.80
4	17.44	0.70	1.31	14.01	11.19	55.35
5	42.32	7.23	2.15	—	—	42.80
6	14.71	2.63	26.13	—	—	56.53

3.3. Discussion

The iron state in hercynite is known to be Fe^{2+}. At high oxygen partial pressure, Fe^{2+} tends to be oxidized to Fe^{3+}. Therefore, Fe^{2+} on the surface of hercynite grains prefers to transform into Fe^{3+} during the sintering process. The main reaction is as follows [17]:

$$4O_2 \rightarrow 4O_o^X + 2V_M^{III} + V_T^{II} + 8h^{\bullet},$$

where O_o^X represents the oxygen atom site; V_M^{III} is the octahedron vacancy with three positive charges; V_T^{II} is the tetahedron vacancy with two positive charges and $h^{\bullet}$ is the electron hole. This reaction increases the concentration of octahedron and tetrahedron vacancies in hercynite lattices. Simultaneously, it further enhances the outward diffusing abilities of Fe and Al ions in crystalline hercynite.

When hercynite crystals contact periclase crystals in magnesia grains, Fe^{2+} (or Fe^{3+}) and Al^{3+} in hercynite diffuse toward periclase because of the concentration difference. At the same time, Mg^{2+} in periclase moves toward hercynite and occupies the oxygen tetrahedron vacancies. This process leads Mg^{2+} to react with Al_2O_3 to form $MgAl_2O_4$. At the same time, Al^{3+} is arrested in hercynite crystals. Therefore, hercynite is transformed into a composite spinel containing a small amount of Fe^{3+} and Fe^{2+}. Because the diffusion rate of Fe^{2+} (or Fe^{3+}) and Al^{3+} toward periclase is faster than that

of Mg^{2+} toward hercynite, composite spinel cavities in hercynite are formed, as shown in Fig. 3(c).

At a sintering temperature of 1600°C, a liquid phase such as CaO·MgO·SiO_2 (CMS) is formed in the CaO–MgO–SiO_2 system because the melting point is only 1500°C [18]. When hercynite grains contact with periclase crystal boundaries in magnesia grains, Fe^{2+} (or Fe^{3+}) and Al^{3+} migrating from hercynite enter the liquid phase through the boundaries. Thus, the boundary liquid phase changes from a CaO–MgO–SiO_2 system to a CaO–MgO–SiO_2–Fe_2O_3–Al_2O_3 system, which further decreases the melting point and viscosity of the boundary liquid [19]. In this study, the CaO/SiO_2 (C/S) mole ratio in the high-purity magnesia is 1–1.2. In Fig. 4, the liquid line in equilibrium with periclase (MgO) at high temperature is marked in red. Fe^{2+} and Al^{3+} ions diffuse gradually from hercynite to the boundary liquid and cause the concentration of Fe^{3+} and Al^{3+} ions in the liquid to be relatively lower than the concentration of Ca^{2+} and Si^{4+}. Meanwhile, Fe^{3+} and Al^{3+} ions have similar effect on the CaO–MgO–SiO_2 system. The phase diagram of the CaO–MgO–SiO_2–10wt%Al_2O_3 system (Fig. 5) was adopted to clarify the influence of Fe^{3+} and Al^{3+}.

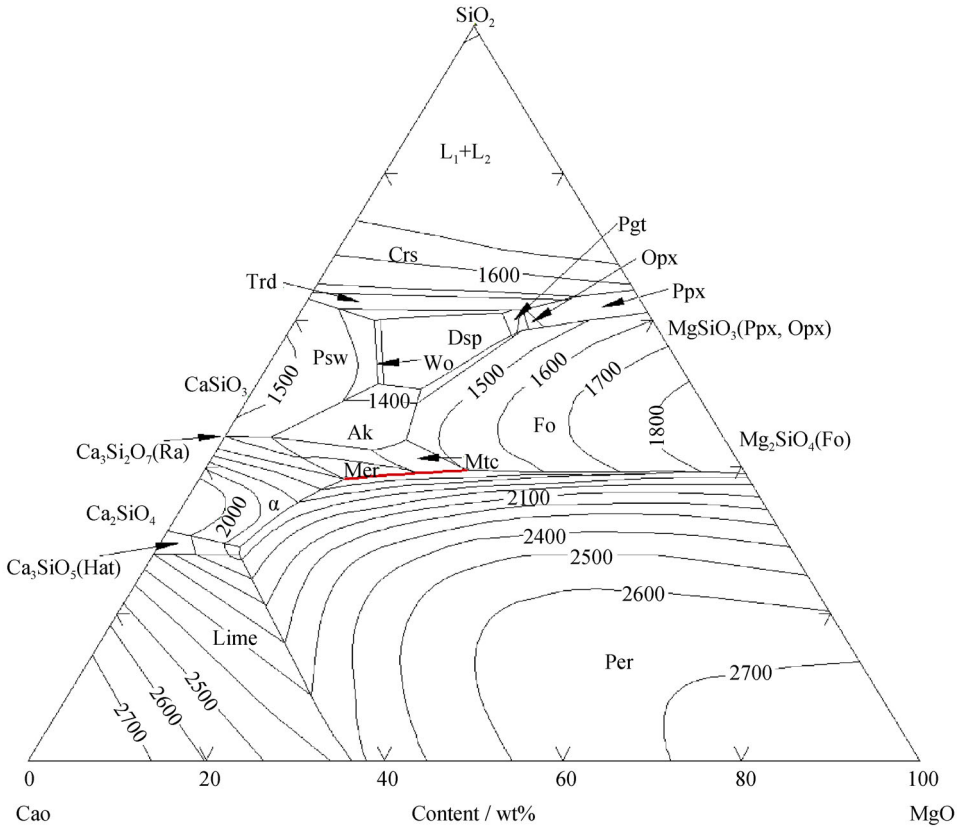

Lime = CaO; Per = periclase; Hat = hatrurite; Ra = rankinite; Psw = pseudowollastonite; Wo = wollastonite; Ak = akermanite ($MgCa_2Si_2O_7$); Mer = merwinite; Mtc = monticellite; Dsp = diaspore; Pgt = pigeonite; Opx = orthopyroxene; Ppx = protopyroxene; Fo = forsterite; Trd = tridymite; Crs = cristobalite; lines represent isotherm at different temperature (°C).

Fig. 4. Phase diagram of the CaO–MgO–SiO_2 system [18].

In view of the phase diagram of CaO–MgO–SiO_2– Al_2O_3 with a low Al_2O_3 content, the phase zones in equilibrium with periclase at high temperature are 2CaO·SiO_2 (C_2S), 3CaO·MgO·2SiO_2 (C_3MS_2), CaO·MgO·SiO_2 (CMS), and 2MgO·SiO_2 (M_2S), which are consistent with the CaO–MgO–SiO_2 system. With respect to magnesia grains, the boundary liquid is in equilibrium with periclase. Therefore, the phases in equilibrium with periclase at high temperature, e.g., 1600°C, are C_2S, C_3MS_2, CMS, and M_2S. The CaO/SiO_2 mole ratio used in this experiment is in the range of 1–1.2. When Al^{3+} enters the boundary liquid at high temperature, the CaO/SiO_2 mole ratio of the boundaries is fundamentally stable; thus, this system is considered to be isolated. The MgO content in the boundary liquid in equilibrium with periclase is between CMS and C_3MS_2. Fe^{3+} and Al^{3+} in the boundary liquid do not belong to the equilibrium composition; they enter the periclase lattices because of the existence of MgO. At the same time, vacancies are formed because of the occurrence of nonequivalent substitution between Fe^{3+}/Al^{3+} and other ions in periclase, which promotes the

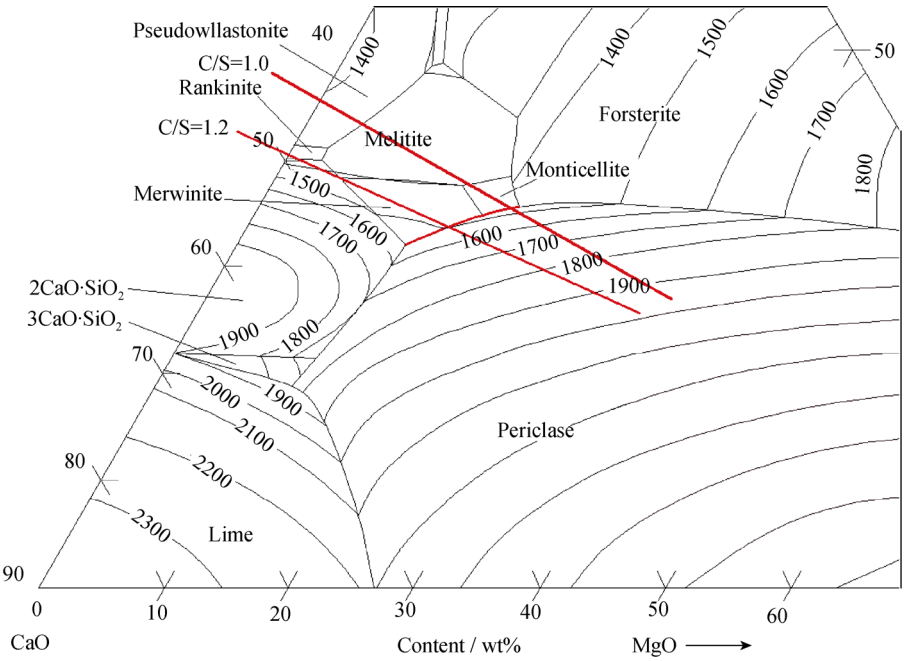

Fig. 5. Phase diagram of the CaO–MgO–SiO_2–10wt%Al_2O_3 system [20] (lines represent isotherm at different temperature (°C)).

diffusion of Fe^{3+} and Al^{3+}. Therefore, a hercynite composite is formed; this composite possesses a high melting point and exists as a solid even at the sintering temperature.

The diffusion rate of Fe^{3+} and Al^{3+} through the boundary liquid is higher than that through periclase crystals because of a lower diffusion energy; thus, the transformation and diffusion of the cations occur primarily in the boundary liquid. Therefore, the spinel composite is initially formed at the boundary instead of at periclase crystals when hercynite contacts magnesia grains.

During cooling, the phase in equilibrium with the main phase (periclase) should possess a composition between CMS and C_3MS_2 without Fe or Al as a consequence of the phase equilibrium. However, the system cannot reach the theoretical equilibrium state in practice; traces of Fe and Al therefore exist in the periclase boundaries, whereas most of the Fe and Al remain in the periclase crystals to form a structure such as that shown in Fig. 3(d).

In the periclase–hercynite brick, in addition to the changes that occur for both magnesia and hercynite grains, similar changes occur for hercynite fine powder in the matrix. Both hercynite and magnesia fines are sintered together at high temperature. A large number of micropores exist, as shown in Figs. 3(c) and 3(d), because of ion diffusion between periclase and hercynite. These features are characteristic of periclase–hercynite bricks prepared from reaction-sintered hercynite and magnesia. At the same time, the micropores contribute to the good thermal shock resistance of the brick.

4. Conclusions

A periclase–hercynite brick was synthesized from magnesia and reaction-sintered hercynite via reaction sintering at 1600°C for 6 h in air. The microstructure evolution of the periclase–hercynite brick before and after sintering was particularly discussed. Some of Fe^{2+} ions in hercynite grains changed into Fe^{3+} ions due to the high oxygen partial pressure. Fe^{2+} (or Fe^{3+}) and Al^{3+} in hercynite migrated toward periclase crystals to form a composite spinel with a high Fe/Al ratio ($(Mg_{1-x}Fe_x)(Fe_{2-y}Al_y)O_4$). Meanwhile, Mg^{2+} in periclase migrated toward hercynite and occupied tetrahedron vacancies. It further reacted with Al_2O_3, forming a spinel-like phase with a low Fe/Al ratio ($(Mg_{1-u}Fe_u)(Fe_{2-v}Al_v)O_4$), whereas Al^{3+} predominately remained in hercynite. The cation diffusion between the periclase and hercynite crystals promoted the sintering process and resulted in the formation of a microporous structure, which contributes to the thermal shock resistance of the periclase–hercynite brick.

Acknowledgements

The authors express their appreciation to the National Nature Science Foundation of China (No. 51172021), the National Science-Technology Support Plan Projects of

China (No. 2013BAF09B01), and the Fundamental Research Funds for the Central Universities (No. FRF–SD–13–006A).

References

[1] D.J. Bray, Toxicity of chromium compounds formed in refractories, *Am. Ceram. Soc. Bull.*, 64(1985), No. 7, p. 1012.

[2] G.P. Liu, N. Li, W. Yan, C.H. Gao, W. Zhou, and Y.Y. Li, Composition and microstructure of a periclase-composite spinel brick used in the burning zone of a cement rotary kiln, *Ceram. Int*., 40(2014), No. 6, p. 8149.

[3] G.B. Qiu, C.S. Yue, X. Li, M. Guo, and M. Zhang, Preparation and characterization of regenerated MgO–CaO refractory bricks sintered under different atmospheres, *Int. J. Miner. Metall. Mater*., 21(2014), No. 12, p. 1233.

[4] W.E. Lee and R.E. Moore, Evolution of *in-situ* refractories in the 20th century, *J. Am. Ceram. Soc*., 81(1998), No. 6, p. 1385.

[5] G.E. Goncalves, A.K. Duarte, and P.O.R.C. Brant, Magneisa-spinel brick for cement rotary kilns, *Am. Ceram. Soc. Bull.*, 72(1993), No. 2, p. 49.

[6] PJ.L. Rodríguez, M.A. Rodríguez, S. De Aza, and P. Pena, Reaction sintering of zircon/dolomite mixtures, *J. Eur. Ceram. Soc*., 21(2001), No. 3, p. 343.

[7] M. Chen, C.Y. Lu, and J.K. Yu, Improvement in performance of MgO–CaO refractories by addition of nano-sized ZrO_2, *J. Eur. Ceram. Soc*., 27(2007), No. 16, p. 4633.

[8] S. Serena, M.A. Sainz, and A. Caballero, The system Clinker–MgO–$CaZrO_3$ and its application to the corrosion behavior of $CaZrO_3$/MgO refractory matrix by clinker, *J. Eur. Ceram. Soc.*, 29(2009), No. 11, p. 2199.

[9] Z.Q. Guo, S. Palco, and M. Rigaud, Bonding of cement clinker onto doloma-based refractories, *J. Am. Ceram. Soc*., 88(2005), No. 6, p. 1481.

[10] J.L. Rodríguez, M.A. Rodríguez, S. De Aza, and P. Pena, Reaction sintering of zircon–dolomite mixtures, *J. Eur. Ceram. Soc*., 21(2001), No. 3, p. 343.

[11] E.A. Rodríguez, G. Alan Castillo, T.K. Das, R. Puente-Ornelas, Y. González, A.M. Arato, and J.A. Aguilar-Martínez, $MgAl_2O_4$ spinel as an effective ceramic bonding in a MgO–$CaZrO_3$ refractory, *J. Eur. Ceram. Soc*., 33(2013), No. 13-14, p. 2767.

[12] J.H. Chen, L.Y. Yu, J.L. Sun, Y. Li, and W.D. Xue, Synthesis of hercynite by reaction sintering, *J. Eur. Ceram. Soc*., 31(2011), No. 3, p. 259.

[13] J. Fukushima, Y. Hayashi, and H. Takizawa, Structure and magnetic properties of $FeAl_2O_4$ synthesized by microwave magnetic field irradiation, *J. Asian Ceram. Soc*., 1(2013), No. 1, p. 41.

[14] Z.Q. Guo and J. Nievoll, Application of magnesia–hercynite refractories in cement rotary kilns, *China Cem*., 2007, No. 5, p. 63.

[15] G.P. Liu, N. Li, W. Yan, G.H. Tao, and Y.Y. Li, Composition and structure of a composite spinel made from magnesia and hercynite, *J. Ceram. Process. Res*., 13(2012), No. 4, p. 480.

[16] T. Yamashita and P. Hayes, Analysis of XPS spectra of Fe^{2+} and Fe^{3+} ions in oxide materials, *App. Surf. Sci*., 254(2008), No. 8, p. 2441.

[17] B. Lavina, F. Princivalle, and A. Della Giusta, Controlled time–temperature oxidation reaction in a synthetic Mg–hercynite, *Phys. Chem. Miner*., 32(2005), No. 2, p. 83.

[18] W.M. Huang, M. Hillert, and X.Z. Wang, Thermodynamic assessment of the CaO–MgO–SiO_2 system, *Metall. Mater. Trans. A*., 26(1995), No. 9, p. 2293.

[19] A. Shankar, M. Görnerup, A.K. Lahiri, and S. Seetharaman, Experimental Investigation of the Viscosities in CaO–SiO_2–MgO–Al_2O_3 and CaO–SiO_2–MgO–Al_2O_3–TiO_2 Slags, *Metall. Mater. Trans. B*., 38(2007), No. 6, p. 911.

[20] E.F. Osborn, R.C. DeVries, K.H. Gee, and H.M. Kraner, Optimum composition of blast furnace slag as deduced from liquidus data for the quaternary system CaO–MgO–Al_2O_3–SiO_2, *Trans. AIME*, 200(1954), No. 6, p. 33.